ELSEVIER

Thermochimica Acta 374 (2001) 55–71

thermochimica acta

www.elsevier.com/locate/tca

Temperature-modulated differential scanning calorimetry: theory and application

Sindee L. Simon*

Department of Chemical Engineering, Texas Tech University, P.O. Box 43121, Lubbock, TX 79409-3121, USA

Received 3 November 2000; received in revised form 21 February 2001; accepted 24 February 2001

Abstract

The status of temperature-modulated differential scanning calorimetry is reviewed, including current methods of data analysis, and the experimental conditions and calibrations necessary for meaningful data interpretation. The theory and application of TMDSC to absolute heat capacity measurements, the glass transition, and crystallization and melting are also reviewed and discussed.

Keywords: TMDSC; ADSC; Temperature-modulated differential scanning calorimetry; Review

1. Introduction

Temperature-modulated differential scanning calorimetry (TMDSC) was introduced in 1993 by Reading under the name modulated DSC [1]. It differs from conventional DSC in that a low-frequency sinusoidal or nonsinusoidal (e.g. sawtooth) perturbation ranging from approximately 0.001 to 0.1 Hz (1000–10 s period) is overlaid on the baseline temperature profile, as shown in Fig. 1 for a sinusoidal perturbation. The use of a complex sawtooth modulation or other complex temperature modulation allows the response to multiple frequencies to be measured at one time [2].

The reported advantages of TMDSC include improved resolution and sensitivity, in addition to being able to separate overlapping phenomena [1,3–6]. In the past 7 years since the commercialization of TMDSC, there has been much work on the theoretical and practical aspects of TMDSC. A literature status was compiled in 1998 [7]. In the current review, an attempt has been made to relay recent findings which impact the application and interpretation of TMDSC.

The paper is organized as follows. The two prevalent data analysis methods are reviewed followed by discussion of the experimental conditions necessary to obtain interprettable data. This is followed by sections on obtaining the heat capacity and the thermal diffusivity from TMDSC measurements. The TMDSC analysis of the glass transition, first-order transitions, and overlapping phenomena are then discussed. The last several sections are devoted to calibration of the temperature, heat flow, and phase angle, respectively.

1.1. Data analysis

The most common TMDSC data analysis involves separating the total heat flow or apparent heat capacity into reversing and non-reversing components. This method was first suggested by Reading [1] and is used by Wunderlich et al. [8] and some commercial

* Corresponding author. Tel.: +1-806-780-1763; fax: +1-806-742-3552.
E-mail address: sindee.simon@coe.ttu.edu (S.L. Simon).

0040-6031/01/$ – see front matter
PII: S0040-6031(01)00493-2

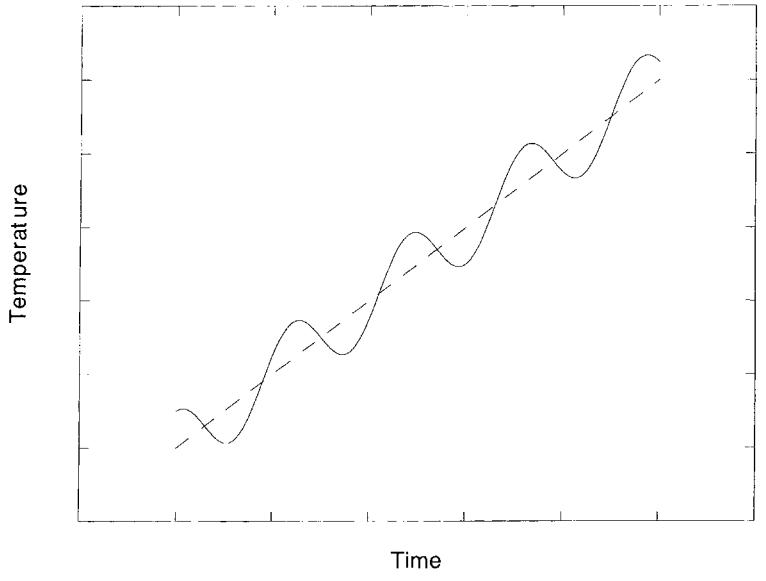

Fig. 1. Typical modulated temperature profile vs. time in TMDSC. The dashed line shows the underlying heating rate.

instrument manufacturers. The reversing component of the heat flow is obtained from the amplitude of the first harmonic of the heat flow, A_p, using a Fourier transform of the data (or an approximation thereof). Dividing by the amplitude of the applied heating rate, $A_{\dot{T}}$, gives the reversing component of the apparent heat capacity

$$C_{p,\text{rev}} = \frac{A_p}{mA_{\dot{T}}} \tag{1}$$

where m is the mass of the sample. The amplitude of the heat flow, A_p, can be measured directly in a power-compensated DSC and can be calculated from the temperature difference between the sample and reference in a heat flux DSC. The applied temperature profile is known which allows $A_{\dot{T}}$ to be calculated assuming that the sample is able to follow the applied temperature profile. For example, for a sinusoidal temperature profile

$$T = T_0 + \beta t + A_T \sin(\omega t) \tag{2}$$

$$A_{\dot{T}} = \omega A_T \tag{3}$$

where β is the heating rate, and A_T and ω are the amplitude and frequency of the perturbation, respectively. T and T_0 are the temperatures of the sample at time t and at time $t = 0$ when the sample follows the applied furnace temperature. Corrections to the heat capacity when the sample is unable to follow the program temperature, for example, due to the effects of thermal resistances and/or finite diffusivity, will be addressed in a later section. The non-reversing heat flow is defined as the difference between the average heat flow $\langle P \rangle$ and the reversing heat flow; the non-reversing heat capacity is the difference between the normalized average heat flow divided by the underlying heating rate β and the reversing heat capacity

$$C_{p,\text{non}} = \frac{\langle P \rangle}{m\beta} - C_{p,\text{rev}} \tag{4}$$

In the absence of thermal events, the reversing heat capacity is simply the frequency-independent heat capacity, C_p and the nonreversing heat capacity is zero. In the presence of thermal events, the reversing heat flow was initially considered to only reflect reversible sensible heat effects (i.e. those due to changes in the heat capacity), and likewise, the non-reversing heat flow was considered to reflect primarily irreversible kinetic effects. The assumption that the sensible heat and kinetic effects can be equated to the reversing and nonreversing heat capacities (or heat flows) is valid only if the kinetics associated with the process being measured are linear and if the kinetic response does not have contributions to the first

harmonic. The assumption breaks down in many circumstances as will be discussed in the sections covering TMDSC analysis of the glass transition and melting.

Another approach to analyzing TMDSC data, suggested by Reading and coworkers [9–11] and advocated by Schawe [12], involves a dynamic heat capacity analysis comprised of the complex, real (storage), and imaginary (loss) heat capacities (C_p^*, C_p', and C_p'')

$$C_p^*(\omega) = C_p'(\omega) - iC_p''(\omega) = \frac{A_P}{A_{\dot{T}}} \tag{5}$$

$$C_p'(\omega) = \frac{A_P}{A_{\dot{T}}} \cos\delta \tag{6}$$

$$C_p''(\omega) = \frac{A_P}{A_{\dot{T}}} \sin\delta \tag{7}$$

where δ is the phase angle between the sinusoidal heat flow and the sinusoidal heating rate. The approach is similar to that used in the dynamic heat spectroscopy measurements pioneered by Birge and Nagel [13,14] and is also only valid if the response is linear [12].

The justification for the existence of a complex heat capacity has been based on fluctuation–dissipation theory and is the subject of considerable work [15–22]. The frequency dependence of the specific heat in an equilibrium (ergodic) system has been variously related to fluctuations in enthalpy [15,16], in temperature [17–19], and in entropy [20], although general agreement has not been reached. Similarly, for TMDSC, the connection of the loss heat capacity with the entropy exchanged [23] or produced [24,25] during a TMDSC cycle has been made. Höhne has criticized this interpretation and has suggested that analogous to other dynamical methods, the loss heat capacity should be associated with the energy dissipated during a cycle [26]. This has been the interpretation of Simon and McKenna [27]. It is most important to note that C_p' and C_p'' originating from fluctuation dissipation theorem are considered to be equilibrium properties; this is not the view of Simon and McKenna [27] regarding the origin of C_p' and C_p'' in the glass transition region. Thermodynamically irreversible processes are not expected to be revealed in equilibrium values of C_p' or in C_p'' [28,29] and the fact that they are (see later) indicates that the dynamic heat capacity measured in TMDSC is a reflection of kinetics rather than thermodynamics. Finally, it should be mentioned that the dynamic heat capacity analysis depends on accurate calibration of the phase angle. The nontrivial task of calibration is discussed in more detail later.

1.2. Experimental conditions

The experimental conditions for operating TMDSC depend on the transitions being measured and have an impact on the reproducibility and meaningfulness of the results obtained. The most important concepts for evaluating the appropriateness of experimental conditions are those of linearity and stationarity [24,25,30–32]. When these conditions are met, the total heat flow in the TMDSC experiment is equivalent to the heat flow from a conventional DSC for the same underlying heating rate.

A linear TMDSC response is one in which doubling the amplitude of the temperature perturbation would double the amplitude of the heat flow. In such a case, the heat capacity given by either Eqs. (1) or (5) will depend only on frequency and not on the amplitude of the perturbation. It has been suggested that the temperature perturbation should be as small as possible to insure linearity [33,34]. However, the increased precision of the TMDSC relative to DSC is due in part to the high instantaneous heating rates [35] with the maximum in the heating rate being given by

$$\left(\frac{\mathrm{d}T}{\mathrm{d}t}\right)_{\max} = \beta + \omega A_T \tag{8}$$

Hence, a more quantitative criteria is warranted.

Merzlyakov and Schick [30] have suggested a criterion for linearity based on the harmonic distortion of the instrument, η

$$\frac{\Delta C_p(\omega)}{C_p(\omega)} = \frac{1}{C_p(\omega)} \frac{\mathrm{d}C_p(\omega)}{\mathrm{d}\dot{T}} A_{\dot{T}} \leq \eta \tag{9}$$

or in terms of the amplitude of the rate of temperature change

$$\frac{\Delta C_p(\omega)}{C_p(\omega)} = \frac{1}{C_p(\omega)} \frac{\mathrm{d}C_p(\omega)}{\mathrm{d}T} A_T \leq \eta \tag{10}$$

where η is approximately 1% for heating rate amplitudes $A_{\dot{T}} = \omega A_T$ from 2 to 60 K min^{-1} [30]. According to these criteria, the maximum allowable amplitude of

the temperature perturbation was reported to be in the millikelvin range for the sharp liquid crystal transition of 4,4′-*n*-octyloxycyanobiphenyl (80CB) and approximately 0.1 K for the melting transition of poly(ether ether ketone) (PEEK) [30]. Application of Eq. (9) by the current author to the glass transition in polystyrene yields a maximum allowable amplitude of the temperature perturbation of 0.6 K through the transition (assuming $C_p = 1.52\ \mathrm{J\ g^{-1}\ K^{-1}}$ in the glass and $\Delta C_p = 0.25$ at the glass transition (both independent of frequency) and that the transition occurs over 10 K)

$$A_{T,T_g} \leq \frac{0.01 C_p}{(\Delta C_p/\Delta T)_{T_g}} \tag{11}$$

where Eq. (11) was obtained by rearranging Eq. (9) and solving for A_T. The maximum allowable amplitudes for linearity through the melt and glass transitions are of the same order of magnitude, but somewhat smaller, than those suggested by Schawe [31]. Note that dC_p/dT in Eq. (9) can be estimated from a standard DSC scan, and $dC_p/d\dot{T}$ in Eq. (10) can be estimated from two standard DSC scans performed at different rates in the range of the instantaneous heating rates of the TMDSC. In both cases, the maximum values of dC_p/dT and $dC_p/d\dot{T}$ should be used in Eqs. (9) and (10) to find the maximum allowable values of A_T and ω for a particular sample.

Stationarity, on the other hand, refers to the sample not changing during a measurement cycle. It is not possible to obtain physically meaningful results from TMDSC (without detailed knowledge of the kinetics of the transformations taking place and mathematical modeling of the response) if stationarity is not maintained [30,31,36]. It is has been suggested that the underlying temperature rate should be low such that the temperature does not change significantly (relative to the temperature perturbation) during a single period [31,37]. However, since it is not known how low is low enough, a quantitative criteria is preferable.

The criteria proposed by Merzlyakov and Shick [30] to insure stationarity depend on how fast the apparent heat capacity changes with time and/or temperature relative to the time of a perturbation period, t_p

$$\frac{\Delta C_p(\omega)}{C_p(\omega)} = t_p \frac{1}{C_p(\omega)} \frac{dC_p(\omega)}{dt} \leq \eta \tag{12}$$

or

$$\frac{\Delta C_p(\omega)}{C_p(\omega)} = \beta t_p \frac{1}{C_p(\omega)} \frac{dC_p(\omega)}{d\langle T\rangle} \leq \eta \tag{13}$$

where $\langle T\rangle$ is the mean temperature. For melting of PEEK, the maximum heating rate for a period of 1 min was reported to be 0.5 K min^{-1} using Eq. (13) with $\eta = 0.02$ [30]. For the glass transition of polystyrene, using the same values as in the previous calculation, Eq. (13) yields a maximum heating rate of 0.6 K min^{-1} for a period of 1 min

$$\beta \leq \eta \frac{C_p}{t_p(\Delta C_p/\Delta T)_{T_g}} = 0.6\ \mathrm{K\ min^{-1}} \tag{14}$$

These results are again comparable to the recommendations made by Schawe; he suggested that the heating rate should be less than 0.7 K/period for the glass transition of polystyrene and 0.2 K/period for the melting transition of poly(ethyleneterephthalate), respectively [31]. Schawe based these recommendations on the criteria that the change in the heat capacity per period should be <0.6 mJ K^{-1} [31]

$$t_p \frac{dC_p(\omega)}{dt} \leq 0.6\ \mathrm{mJ\ K^{-1}} \tag{15}$$

This is again comparable but slightly higher than the criteria of Eq. (12) for typical values of C_p and for $\eta = 0.02$ which yields approximately 0.3 mJ K^{-1}. The issue of stationarity has also been addressed by Snyder and Mopsik for dielectric measurements through a transition during a temperature ramp [38].

It is very important that the specifics of the transition being measured are accounted by using Eqs. (12) (13) or (15) rather than using a standard recommendation. For example, simulation results obtained by Di Lorenzo and Wunderlich [39] showed that sharp crystallization exotherms resulted in artifacts in the reversing heat flow. Using Eq. (13) and the data presented from Fig. 1 of [39] [$mC_p \approx 1.3$ J/K, $\beta = 1$ K min^{-1}, $t_p = 60$ s, and calculating $(dP/dt)_{max}$], the change in the heat flow due to non-stationarity is calculated to be <2% for the case where there were artifacts only slightly larger than expected noise in the reversing heat flow and >4% for the cases where significant artifacts were present. This appears consistent with Merzlyakov and Schick's suggestion that the maximum harmonic distortion should be <0.01 or 0.02.

In addition to insuring that linearity and stationarity are met by determining the maximum allowable values of the experimental parameters, A_T, ω, and β, using Eqs. (9), (10), (12) and (13), it is important that steady state is also reached before collecting data [35,40,41]. For quasi-isothermal measurements (in which $\beta = 0$), steady state can be confirmed by insuring that the Lissajous loops are reproducible. Lissajous loops can be made by plotting modulating heat flow versus modulating temperature or by plotting heat flow versus the modulating heating rate. For quasi-isothermal experiments, the loops should be invariant after steady state is reached. For non-isothermal experiments, the loops should be elliptical and symmetric about the axes [35,41]. In addition, there are instrumental limitations for the minimum values of the experimental parameter of A_T related to the sensitivity of the instrument. For example, heat flow amplitudes of <100 μW are generally not recommended; this heat flow minimum corresponds to a minimum temperature amplitude of approximately 0.1 K when the period is 60 s for most polymers.

1.3. Absolute heat capacity measurements

One of the reported advantages of TMDSC initially was the ability to measure the absolute heat capacity without the need to make multiple runs. Theoretically, if there were no thermal resistances and if the sample thermal diffusivity were high enough, the sample and reference would both follow the applied temperature profile exactly and Eq. (1) would give the frequency independent heat capacity in regions away from any transitions. (Eqs. (5) and (6) could also be used with the same result since away from any transitions and with no thermal lag, δ is expected to be zero.) In reality, however, the effects of both sample thermal diffusivity and thermal resistances must be first taken into account. These effects result in the apparent or measured heat capacity being lower than the actual heat capacity.

In order to obtain accurate heat capacity measurements, the sample must be thin enough that the entire sample experiences the maximum applied temperature perturbation [41–43]. According to a derivation by Hatta and Minakov which neglects thermal contact resistances, when the thermal diffusion length is approximately <40% of the sample thickness, L, the sample will follow the applied temperature perturbation closely enough that the heat capacity is accurate to within 1% [44]. Their criteria, then, in the absence of thermal contact resistance can be written

$$\sqrt{\frac{\omega}{2k}}L \leq 0.4 \tag{16}$$

where k is the thermal diffusivity ($=\kappa/\rho C_p$, where κ is the thermal conductivity, ρ the density, and C_p the heat capacity). For a sapphire sample, the maximum thickness was calculated to be 0.7 cm, whereas for polystyrene, the maximum thickness was found to be 0.06 cm [31]. The criteria for sample thickness is consistent with the recent experimental work of Androsch and coworkers who measured the thermal gradient in DSC samples with and without lids [45]. It is also consistent with calculations by Simon and McKenna [46] which were based on a sample encapsulated in an alumnium pan, the latter of which was assumed to be a perfect conductor effectively dividing the sample thickness in half. From those calculations, the maximum sample thickness to obtain the heat capacity within 1% is twice that calculated by Hatta and Minokov (e.g. 0.12 cm for polystyrene) as might be expected due to the assumption of the effect of the aluminum pan. It is noted that the recent work of Androsch and coworkers supports our assumption that the aluminum pan is a perfect conductor [45]. Eq. (16) is also consistent with the results of Schenker and Stager [47] and the work of Buehler and Sefaris [48].

In addition to insuring samples are thin enough, the effects of thermal contact resistance have to be taken into account in order to obtain accurate heat capacities. This is where instrument calibration and modeling of the thermal resistances becomes important. Wunderlich reported that the heat capacity calibration constant, defined as the ratio of the literature heat capacity to the measured heat capacity, for sapphire and polystyrene samples in a heat-flux TMDSC depended in a complex way on temperature, frequency, cell imbalance, mass of the sample and pan type [41,42]. There was only a slight effect on the amplitude of the temperature perturbation. The dependence on sample mass was originally suggested to be due to thermal diffusivity effects, but since the sample thickness met the criteria discussed above, Hatta and Minakov [44] suggested that it might instead be due to changes in the thermal contact resistance. Schawe and

Winter similarly found a complex dependence of the calibration constant on frequency, sample geometry, and thermal contact resistance for measurements in power-compensated TMDSC [49]. However, in spite of the complex dependence of the calibration constant on experimental parameter, Varma-Nair and Wunderlich were able to obtain the heat capacities of polystyrene, quartz, and lube oil to within several percent using standard pans [41]. The measured heat capacities of water, heptadecane, and lube oil sealed in hermetic pans, on the other hand, were in error by 3–14%, indicating that hermetic pans should not be used for absolute heat capacity determinations [41]. Other researchers have found similar problems with hermetic pans [50].

Despite the good results with standard pans, however, it is not very satisfactory that the heat capacity calibration constant depends so strongly on the experimental parameters. An explanation may be found by modeling the TMDSC experiment. Two approaches to modeling have been performed. One is to solve the boundary value problem consisting of the general heat conduction differential equation, which for temperature variations only in the axial direction, x, is

$$k\frac{\partial^2 T}{\partial x^2} = \frac{\partial T}{\partial t} \tag{18}$$

where k is the thermal diffusivity. This equation is solved with boundary and initial conditions to obtain the temperature gradients inside the sample [44,46–49,51–53], which are then usually related back to the steady state heat flow by neglecting the transient terms and using a heat balance. We note that Buehler and Seferis [48] numerically solved the three-dimensional boundary value problem rather than the one-dimensional problem. The effects of heat transfer limitations were incorporated by several researchers [46,49,52]. Using this approach (including the heat transfer effects), Schawe and Winter were able to quantitatively describe the experimental dependence of the calibration factor on frequency for samples of various geometries [49]. The boundary value solution also predicts no dependence of the calibration factor on amplitude of the temperature perturbation in agreement with experimental results [41,49,54]. The dependence of the heat capacity calibration factor on temperature can be attributed to the dependence of the thermal diffusivity and the heat transfer coefficient on temperature.

The alternate approach to modeling TMDSC invokes an electrical analogue in which thermal contact resistances are modeled as resistors and the heat capacity of the sample is modeled as a capacitance [44,53,55,56]. The simplest model of the TMDSC sample assumes only a resistance between the sample and the baseplate in series with a capacitance and yields a relationship between the apparent or measured heat capacity, C_{app}, and the actual heat capacity, C_p

$$\frac{C_{\text{app}}}{C_p} = \frac{1}{(1+\omega^2\tau^2)^{1/2}} \tag{19}$$

where τ is a time constant ($=mR_{\text{th}}C_p$ where R_{th} is the thermal resistance in K W^{-1}). The solution is mathematically equivalent to that derived by Wunderlich and coworkers [35] except that the time constant in Wunderlich's solution depended on the heat capacity of the empty pan rather than of the sample. A more realistic analogue, which results in a more complicated expression involving two relaxation times, includes resistances between the thermal bath and ovens (or baseplate) on both sample and reference sides and another resistance between the pan and sample with the heat capacities of both the sample and the oven or baseplate accounted for [44,55]. The model is yet more complicated if a reference pan is included [53], and hence it has been suggested that calibration is simpler if the reference pan is not used [44]. Wunderlich and coworkers have intimated the same [35]. Cao has done an analysis similar to Wunderlich's (neglecting thermal gradients) and reported that the calibration constant also depends on frequency and the heat capacity of the reference [57].

An important point to note when contrasting the two approaches to modeling TMDSC is that although both approaches predict a frequency dependence of the measured heat capacity, the electrical analogue does not account for the finite diffusivity of the sample. Höhne has discussed this issue and noted that for thicker samples the electrical analogue will not give the right correction for the heat capacity [53,55]. This is also the case for thin samples at high frequencies. A comparison of the two modeling approaches has been made by the author and is shown in Fig. 2. In the figure, the points are the solutions to the boundary value problem for polystyrene for two values of sample thickness L and for two values of the dimensionless

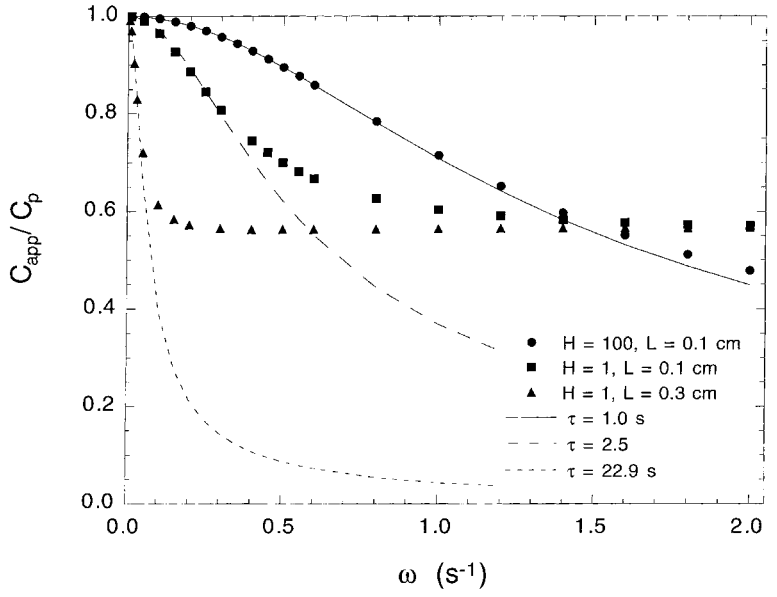

Fig. 2. Ratio of apparent heat capacity to actual heat capacity as a function of frequency for three simulated conditions. The symbols show the calculations based on solution of the full boundary value (BV) problem Eq. (18). The lines show that the electrical analogy Eq. (19) is valid only at low frequencies and that the limit of its validity depend on sample thickness (L) and the heat transfer coefficient (H).

heat transfer coefficient ($H = ah\kappa^{-1}L^{-1}$, where h is the heat transfer coefficient with units of W K^{-1} m^{-2} and a is the area of heat transfer). The solution presented is that reported previously by Simon and McKenna [46]. The electrical analogue given by Eq. (19) is shown by the lines in Fig. 2. It can be seen that the electrical analogue is only a good approximation of the boundary value solutions at low frequencies. The specific frequency above which the electrical analogue is not valid depends on the value of the heat transfer coefficient and the sample thickness, with poorer heat transfer and thicker samples resulting in deviation at between the boundary value solution and the electrical analogue at lower frequencies.

At low enough frequencies and/or for thin enough samples, the heat capacity calibration constant is unity for both models. Experimentally, this is found to be the case for DSCs with symmetrical or balanced sample cells if the sample and reference pans have the same weight [41,48]. If, on the other hand, the DSC cells have a large imbalance (i.e. the apparent heat capacity is significant when running the empty calorimeter), then the measured heat capacity must be corrected by subtracting (or adding depending on the bias) the baseline heat capacity obtained using pans of matching weights [41] in addition to corrections using the frequency dependent calibration factor.

1.4. Thermal diffusivity measurements

The fact that the apparent heat capacity decreases with sample thickness due to the finite thermal diffusivity of the material is the basis for measuring thermal diffusivity by TMDSC [58]. However, the resistances to heat transfer also affect the apparent heat capacity, as described in the previous section, and for that reason, Simon and McKenna [46] concluded on the basis of solutions to the general heat conduction equation that the frequency dependence of C_{app}/C_p could not be used to accurately obtain the thermal diffusivity of the sample unless the heat transfer coefficient was already known.

However, Merzlyakov and Schick have recently shown that the effects of thermal diffusivity and heat transfer can be separated using the storage and loss heat capacities since the shape of the crossplot of the two components depends only on the heat transfer coefficient [59]. Cole–Cole plots based on the previous calculations of Simon and McKenna confirm

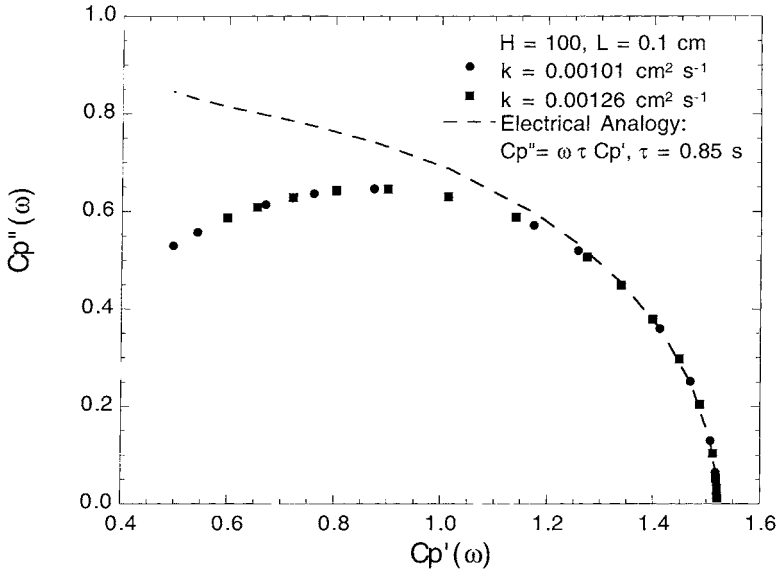

Fig. 3. Cole–Cole plot of the loss vs. the storage heat capacity for simulated data generated by solution of the boundary value problem Eq. (18). $H = 100$ and $L = 0.1$ cm for the simulations. The symbols show the behavior for different values of the thermal diffusivity, k. The dashed line shows the electrical analogy.

this result. Fig. 3 shows the crossplot of the loss versus storage heat capacities with data obtained from our previous solution [46] of the boundary value problem for heat conduction for $H = 100$ and $L = 0.1$ cm for a thin encapsulated polystyrene sample. Two solutions are shown corresponding to two values of the thermal diffusivity k. As Merzlyakov and Schick pointed out, the two solutions give the same shape allowing H to be determined from a fit of the curvature. Once H is determined, k can be calculated from the dependence of C_{app}/C_p on frequency [46]. Also plotted for illustration purposes in Fig. 3 is the expected curvature based on the electrical analogue with one relaxation time which gives $C_p' = \omega\tau C_p''$. The breakdown of the electrical analogue at high frequencies is even more apparent in this plot than in Fig. 2. The primary difficulty using the above methodology to find H lies in correctly calibrating the phase angle between the heat flow and the rate of temperature change. This is addressed in the calibration section.

1.5. TMDSC and the glass transition

Before discussing the use of TMDSC to characterize the glass temperature (T_g) and associated kinetics, the enthalpy (H) versus temperature (T) behavior in the vicinity of T_g is briefly reviewed. Many reviews of the glass transition have been written, including [60–63]. At high temperatures the material is at equilibrium. During cooling from equilibrium, the enthalpy decreases and the molecular mobility of the material decrease. At the glass temperature (T_g), the material is no longer able to maintain equilibrium in the time scale of cooling and the enthalpy departs from the equilibrium line and moves onto the glass line. The solid curve in Fig. 4a shows this behavior schematically. It is important to understand that this departure from the equilibrium line depends on the rate of cooling. A faster cooling rate results in departure from equilibrium at a higher temperature. This also means that T_g is frequency dependent, and thus, is expected to depend on the modulation period in TMDSC. The frequency dependence of the calorimetric T_g has been demonstrated experimentally by TMDSC [25,29,64–72], as well as by the 3-ω dynamic heat spectroscopy method [13,14,18,19,24].

Still referring to Fig. 4a, we now look at what happens to the enthalpy during heating without modulation. For an unaged glass, i.e. if no relaxation occurs isothermally in the glassy state or during

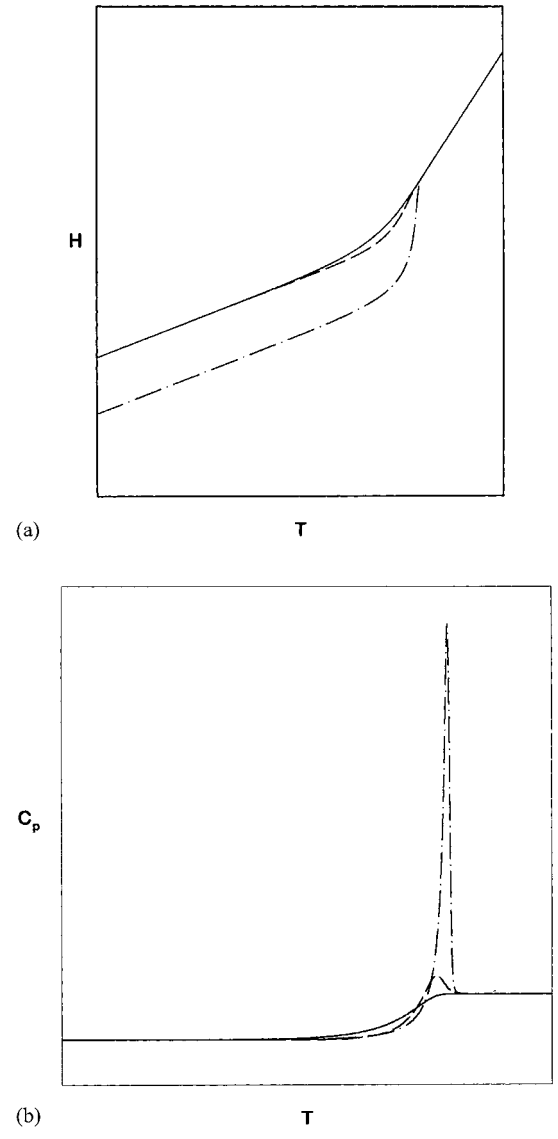

Fig. 4. (a) Schematic of enthalpy vs. temperature behavior. The solid line shows the response on cooling. The behavior on heating is shown for both an unaged glass (dashed line) and for an aged glass (dash-dot line). (b) Schematic of heat capacity vs. temperature behavior for curves corresponding to those shown in (a). The solid line shows the response on cooling. The behavior on heating is shown for both an unaged glass (dashed line) and for an aged glass (dash-dot line).

heating, the dashed curve is observed during heating. Some small hysteresis in the vicinity of T_g is observed between the cooling and heating scans. On the other hand, the dash-dot line shows the behavior on heating of an aged glass. Since the aged glass has lower molecular mobility (corresponding to its increased density), the enthalpy often overshoots the equilibrium line during heating such that the rapid increase to equilibrium occurs at a temperature considerably above the glass temperature, as shown. The corresponding heat flow (P) or apparent heat capacity (C_p) for the aged and unaged glasses is shown in Fig. 4b. For the unaged material, there is simply an endothermic step change in the heat flow at T_g. For the aged glass, an annealing peak is observed. The difference between the area under the ideal curve and that of the aged glass is the difference in enthalpy between the glass lines for the unaged and aged glasses (ΔH_a) [73]. In traditional DSC, ΔH_a is obtained by performing a temperature scan for an aged glass to obtain the aged response, then quenching the material at a given rate, and performing a second temperature scan without aging the material to obtain the unaged response. A purported advantage of TMDSC is the ability to separate the enthalpy relaxation from the reversing heat capacity [1,3,4], and thereby, possibly obtain the same information with only one temperature scan.

A typical TMDSC scan with total, reversing, and nonreversing heat flows, is shown in Fig. 5. This scan was simulated using the Tool–Narayanaswamy–Moynihan (TNM) model of structural recovery [74,75] which has been shown to describe the glass transition and associated kinetics well. The midpoint in the step change of the reversing heat flow can be defined as $T_{g,rev}$ and if the assumptions underlying the TMDSC analysis are appropriate, this value should be comparable to the value of T_g obtained in a linear experiment as a function of frequency. In fact in simulations of TMDSC through the glass transition using the TNM model, Simon and McKenna [76] found that $T_{g,rev}$ is within 1.0°C of the expected T_g for experimental conditions where there are at least 4 cycles through the transition, in spite of the fact that the kinetics associated with the glass transition are nonlinear [51,62,63,74,75]. This is consistent with Schawe's results that suggest that the linear response approach is valid for the glass transition for modulation amplitudes up to 1.5 K for polystyrene [77], as well as with the experimental work of Boller et al. [65]. The latter researchers reported that the glass transition temperature of polystyrene could be measured on heating in TMDSC and that it depended on the modulation

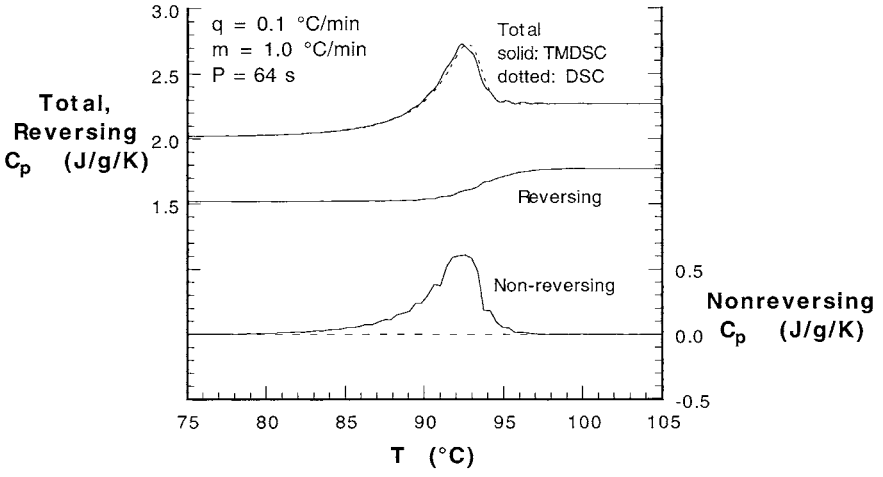

Fig. 5. Simulated TMDSC total, reversing, and nonreversing signals, in heat capacity units, for aged polystyrene. The total heat capacity is offset by 0.5 J g^{-1} K^{-1} for clarity. The results of the analogous unmodulated DSC simulation are also shown.

period and only weakly on the thermal history or degree of aging of the sample. Wunderlich and Okazaki subsequently pointed out that the differences between the reversing heat flow measured on cooling and heating could be decreased by going to smaller underlying heating rates and were the same in the limit of quasi-isothermal measurements [78]. Schick and coworkers have similarly suggested that to obtain only the frequency dependence of the glass transition without cooling rate effects, it is necessary to have the cooling rate slow enough that an unmodulated scan would show only the liquid equilibrium response and no transition in the region of frequency-induced transition [79]. The quasi-isothermal response meets this criteria. Since annealing peaks can occur up to 20 or 30°C above T_g giving erroneously high values of T_g if corrections are not made, TMDSC is a practical and useful tool for obtaining T_g.

The enthalpy change due to relaxation or aging below T_g is also often of interest, particularly to researchers interested in the kinetics associated with the glass transition. It was initially suggested that the nonreversing heat flow, ΔH_{non}, contains information related to the enthalpy relaxation experienced by the sample. In fact, the area of the peak in the nonreversing heat flow was equated to the enthalpy change during isothermal aging, ΔH_a, in early work on TMDSC [80]. However, Simon and McKenna have since been pointed out that the kinetics associated with enthalpy recovery are nonlinear, and that care must be taken in interpretting the nonreversing heat flow [51]. Reading and Luyt reported that the nonreversing heat flow was not directly related to ΔH_a particularly for long aging times [132]. This was confirmed by Hutchinson and coworkers compared the ability to obtain ΔH_a from TMDSC and DSC [81]. The enthalpy change due to isothermal aging, ΔH_a, was measured by DSC using two temperature scans of the aged and unaged glass, respectively, ($\Delta H_a = \Delta H_{aged} - \Delta H_{unaged}$ [81]), whereas it was measured by TMDSC by subtracting the nonreversing heat flow obtained in the cooling scan of the unaged material from that obtained during heating scan of the aged material ($\Delta H_a = \Delta H_{non,aged} - H_{non,unaged}$). The TMDSC ΔH_a was within 0.5 J/g of the DSC value except at long aging times where the result was worse. A slight improvement was found if the TMDSC total heat flows rather than the nonreversing heat flows were used to calculated ΔH_a. Hutchinson's conclusion was that since DSC can be used to measure ΔH_a to better than 0.5 J/g, DSC rather than TMDSC should be used for quantitative determination of ΔH_a. Simon and McKenna came to a similar conclusion based on TNM simulations of the glass transition [76]. In that work, we found that the error in equating the nonreversing heat flow to ΔH_a arises from three sources: enthalpy undershoots, contributions of structural recovery to the first harmonic and/or contributions

of the step change at T_g to higher harmonics, and interactions between the dynamic measurements made during a temperature ramp when a low frequency probe is coupled with a high scanning rate. Although, the third source can be eliminated by insuring the conditions of linearity using the criteria of Merzlyakov and Schick [30] as described previously and the first source can be minimized by insuring that undershoots are not present (i.e. ΔC_p from the total and reversing heat flows are identical), the second source is not controllable and results in errors in ΔH_a obtained from TMDSC that are larger than those incurred with conventional DSC. [76] Without using a nonlinear model to extract ΔH_a from TMDSC data, it has to be concluded, in agreement with Hutchinson, that the conventional methodology using DSC is better. Bailey et al. have recently come to a similar conclusion [82].

In addition, C_p'' in the glass transition regime has been found by Hutchinson and Montserrat [83] to be essentially independent of the enthalpic state of the glass except for relatively high degrees of aging (large excess enthalpy). This result is not surprising and is consistent with earlier work by other researchers [29]. The result supports the assumption that the first harmonic is generally dominated by the sensible heat term. This is, in fact, why T_g can be measured relatively accurately on heating in TMDSC using either C_p' or the reversing heat flow. However, the fact that there are contributions of structural recovery to the first harmonic and/or contributions of the sensible heat to the higher harmonics results in the inability to measure ΔH_a from the nonreversing heat flow as discussed above.

1.6. Melting and crystallization

First-order transitions, such as crystallization, melting, and liquid crystal transitions, have been investigated by TMDSC and this has led to both a better understanding of the melting of polymer crystals and a better understanding of TMDSC. It cannot be emphasized enough, however, that the conditions of linearity and stationarity must be maintained during first-order transitions. Due to the nonlinearity of the melting process and the sometimes large latent heats, this can be difficult to achieve. If linearity is not maintained, the resulting distortions in the reversing and nonreversing heat flows and/or the dynamic storage and loss heat capacities may severely compromise interpretation of the results. Schawe and Strobl explain in detail the steps they take to insure linearity in their measurements through the melting transition [84]. In addition, Höhne [85] has stressed that it is essential to separate time-dependent melting and heat transfer effects; again, this can be more difficult when large amounts of heat must be transferred during the transition. It should be remembered that melting takes time and the sample temperature remains constant during melting (for simple materials having one melting temperature); hence, the temperature of the sample may not follow the program temperature through the melting transition.

We need to distinguish now between reversible first-order transitions, in which there is little superheating and supercooling, and transitions which are essentially irreversible with respect to the temperature changes incurred during a TMDSC period [86,87]. Metals and nucleated liquid crystals display reversible or nearly reversible melting (e.g. indium superheats by <0.1 K and supercools by approximately 1 K [88]), whereas polymers lie at the other end of the spectrum with respect to the reversibility of their melting and crystallization due in part to the strong temperature dependence of the nucleation process. In addition, polymer melting is complicated by fast kinetics, the coexistance of crystallization and reorganization, and the wide distribution of equilibrium melting points [89]. The coexistance of crystallization and reorganization during melting can lead to a degree of reversibility in the melting of many polymers as indicated by the presence of a reversing component of the melting peak and/or by the presence of a peak (or peaks) in the dynamic heat capacities and in the phase angle [3,86,87,90–99]. Before going into more detail on this point, however, let us back up and review the TMDSC response of materials that exhibit reversible or nearly reversible melting and crystallization.

For materials with negligible supercooling and superheating, melting and crystallization both can occur in a single modulation cycle at temperatures in the vicinity of the melting point (T_m). Melting occurs when the temperature rises above the melting point, followed by crystallization if the temperature falls below the melting point in the same cycle. The reversing and dynamic heat capacities might be

expected to remain relatively constant through the first-order melting transition since the heat capacity itself does not change appreciably through the transition. However, peaks are observed in these quantities during melting of metal standards. The peak in the reversing heat flow arises because the reversing heat flow is calculated only from the amplitude of the heat flow, and the amplitude (which is indifferent to the sign of the heat flow) increases when melting and crystallization take place in the same modulation cycle [86]. The peaks in the dynamic heat capacities arises from the same phenomena since they also depend on the amplitude of the heat flow [100]. The magnitude of the peaks in the reversing heat capacity is not related to the heat of fusion or to changes in the sensible heat or heat capacity. In fact, the area of the reversing heat flow is larger than that of the total heat flow due to recrystallization and remelting. The heat of fusion and the degree of melting that takes place per cycle can only be obtained from the total heat flow by subtracting the baseline modulating heat flow due to sensible heat effects (C_p) and then integrating the resulting curve to obtain the endothermic and exothermic heat flow for each cycle [86,87,101]. The heat of fusion equals the difference between the sum of all endotherms and the sum of all exotherms through the transition region [87,101]. Fig. 6 shows the TMDSC total heat flow response for reversible melting of indium with the excess exothermic (crystallization) and endothermic

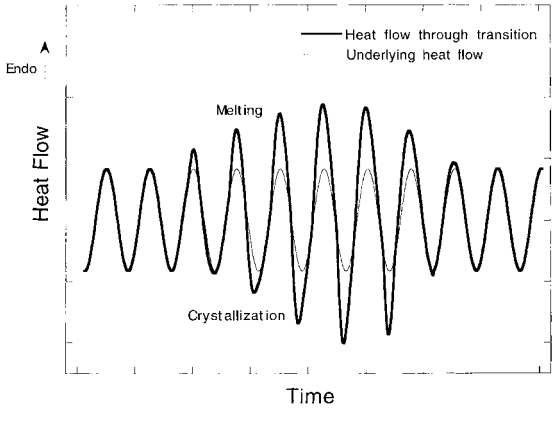

Fig. 6. Schematic of modulated heat flow vs. time through a reversible first-order transition. The integrated difference between the heat flow (thick line) and the underlying heat flow (thin line) is ΔH_m.

(melting) heats indicated. Applying the condition of heating only, in which

$$\left(\frac{dT}{dt}\right)_{min} = \beta - \omega A_T > 0$$

simplifies the TMDSC response because it eliminates the possibility for reversible melting and crystallization [102].

Polymeric crystals often show negligible reversibility during the melt transition, particularly for "perfect" crystals formed by slow cooling [86,87]. Models of irreversible melting of polymer crystals are able to explain the dependence of the apparent heat capacity on frequency, heating rate in experiments having an underlying heat rate, and time in quasi-isothermal experiments [100,103–105]. However, as has already been alluded to, reorganization and recrystallization (i.e. reversible melting) has been observed during the melting transition of many polymers [3,86,87,90–99]. The TMDSC, thus, has provided new insight into polymer crystal melting.

Crystallization of materials has also been studied by TMDSC. Toda has related the change in the phase angle during crystallization of several polymers to the crystal growth rate [106–108]. In those works, the temperature dependence of the growth rate measured by TMDSC was found to agree with that obtained from optical measurements. During isothermal crystallization, one might expect the heat capacity of the material to decrease since the heat capacity of the crystal is lower than that of the amorphous material. Although this is generally found to be the case, the heat capacity does not always decrease to the value expected based on the degree of crystallinity [109]. For example, Schick et al. examined the evolution of the dynamic or reversing heat capacity during isothermal crystallization of both a low molecular weight and a polymeric compound [110]. They found that for the low molecular weight compound, the heat capacity decreased as expected during crystallization to the value of the heat capacity of the crystal phase. On the other hand, the heat capacity of the semicrystalline polymer levelled off at a value considerably above that expected based on the degree of crystallinity. This excess heat capacity was calculated to correspond to a small change in crystallinity, on the order of 0.2% out of a total crystallinity of 50%, during a single perturbation cycle. Similar to the new knowledge gained by

crystallization and reorganization of polymer crystals during melting, reversible melting during crystallization may be expected to provide new insights into polymer crystallization behavior.

1.7. Separation of overlapping transitions

Temperature-modulated DSC has found considerable use in the study of thermoset cure. During the curing process, the glass transition temperature of the material increases as monomer is converted to polymer by chemical reaction. If the isothermal cure temperature is low enough, T_g will rise above the cure temperature, the material will vitrify, and the reaction may become diffusion controlled depending on the timescale of diffusion relative to that of reaction [111,112]. Van Mele and coworkers have found quasi-isothermal TMDSC useful for studying this process since in TMDSC, the reversing heat capacity shows the vitrification process as a step change from the liquid heat capacity to the glassy heat capacity, whereas the nonreversing heat flow, on the other hand, yields the heat of reaction [113]. Knowing the point of vitrification during quasi-isothermal cure gives researchers an indication of where the kinetic reaction model may break down and where diffusion control may become important. It must be kept in mind, however, that diffusion control may start well before vitrification for very fast reactions and well after vitrification for very slow reactions [112]. Consequently, the use of a mobility factor [113,114] derived from the normalized decay in the heat capacity to describe the effect of diffusion on the reaction rate is not applicable to all thermoset reactions.

In addition to vitrification and the heat of reaction, during a TMDSC temperature scan, devitrification is also observed [115]. The TTT and CHT isothermal cure diagrams of Gillham [111,116] can easily be constructed from quasi-isothermal and ramp TMDSC studies, respectively [117]. Reaction-induced phase separation during thermoset cure has also been studied by TMDSC, [118–121] as has the autoacceleration effect in a free radical crosslinking system [122]. The TMDSC has also been used to study phase separation and devitrification in sol–gel glasses [123].

In other TMDSC applications involving overlapping transitions, the characterization of interpenetrating networks [124–127] and polymer blends [128] has been reported. Hourston and coworkers have developed a methodology using the temperature derivative of the heat capacity during a transition coupled with knowledge of ΔC_p for the components in their interpenetrating networks to estimate the weight fraction and degree of mixing of various phases [124–126]. In work by other researchers in which one of the phases in the intepentrating network was semicrystalline, it was necessary to subtract the contribution of melting from the heat flow in order to observe the glass transition of the other phase [127].

1.8. Calibration of temperature

Calibration of temperature in TMDSC can be accomplished in several ways. Hensel and Schick found that the calibration can be performed in normal DSC mode with extrapolation to zero heating rate yielding errors of <0.2 K for heating rates <1 K min^{-1} [129]. These researchers [129], as well as Wunderlich and coworkers [101], have also suggested the use of various liquid crystalline transitions for TMDSC temperature calibration in the TMDSC mode for liquid crystalline transitions that do not show supercooling. Alternatively, the temperature calibration can be performed using standard metal melting samples and quasi-isothermal experiments (in which the underlying heating rate, β, is zero) due to the sharpness of the transition and the reversible nature of metal melting. By performing quasi-isothermal experiments at various temperatures using small modulation amplitudes, the temperature (plus or minus the temperature modulation amplitude) at which melting first occurs can be determined and used as the temperature calibration [101]. The TMDSC temperature calibration should not be accomplished during a modulated temperature scan because of the nonlinearity associated with the melting of conventional metal standards [129,130].

1.9. Calibration of heat flow

The calibration of the heat flow for TMDSC experiments can also be performed in the conventional DSC mode. Wunderlich, for example, calibrated the heat flow using indium in the conventional way, and then found that the heat of a liquid crystalline transition was within 2% of that measured by conventional DSC [101]. However, since the heat of transition must be

determined from the time domain data after subtracting the underlying sinusoidal component, it is considerably easier to calibrate heat flow in the conventional DSC mode.

There are many papers that discuss calibration of the heat capacity of the heat flow amplitude in conjunction with absolute heat capacity measurement [35,41,42,50,53,131]. When the heat flow is calibrated using standard methods, then the measured heat capacity will depend on frequency and sample size due to the thermal gradient effects as shown in Fig. 2 and discussed above. Rather than calibrating the heat capacity (or heat flow amplitude) for these effects which are inherent in the TMDSC response and give additional information, it is more reasonable if one wants absolute heat capacity to use thin samples in which thermal gradients are not a problem and to simply calibrate the heat flow in the conventional way.

1.10. Calibration of phase angle

In the absence of thermal events, the ideal TMDSC response would give the heat capacity and zero phase lag. However, as already discussed, the TMDSC is not ideal. There are heat transfer effects in the sample, as well as resistances and asymmetries in the instrument itself, which result in measured phase lags. The simplest method of correcting for instrument effects is a linear [9] or sigmoidal interpolation [132]. Theoretical justification has been given [51]. On the other hand, since to a first approximation, the phase angle scales with the heat capacity ($C_{p,\mathrm{rev}}$ or C_P^*) [8], Schick and coworkers suggested that scaling and inverting the heat capacity so that it matches the measured phase angle before and after the transition of interest provides a baseline for the phase angle [133]. Subtracting the baseline phase angle (f_{baseline}) from the measured phase angle (f_{exp}) gives the corrected phase angle

$$\phi = \phi_{\mathrm{exp}} - \phi_{\mathrm{baseline}}$$

Support for the Schick's approach and for the expected dependence of the phase lag on frequency [8] in the glass transition regime was reported by Hutchinson and coworkers [134] based on experiments using thin samples. It is noted that the approach implicitly assumes that the heat transfer coefficient and thermal gradient in the sample is not changing significantly during the thermal event [49]. This may not be the case, particularly for thick samples, since, for example, the heat transfer coefficient and the thermal diffusivity can change through the glass and melting transitions. Use of a thin layer of oil or grease between the sample and the pan can minimize changes in heat transfer [30,135], however, the changes in thermal diffusivity through transitions are difficult to account for without solving the boundary value problem. Rather, care must be taken that samples are thin enough that thermal gradients are negligible as previously discussed. For the melting transition, where the heat capacity does not change significantly during the transition, simply equating the phase angle baseline to the measured phase angle before and after the transition has given good results [102].

Recently a procedure for correcting the heat flow and the phase angle has been developed by Höhne, Merzliakov and Schick [53]. The method involves determining the response of the DSC to a small step change in temperature. The response to the temperature pulse for two empty pans of identical weight is subtracted to the response obtained for the sample in order to account for instrument asymmetries. The Fourier transform of the normalized response yields the magnitude and phase of the transform function which can then be used to correct both the measured heat capacity and phase angle. A more complicated calibration procedure along the same lines can be performed to separate the sample and instrument effects [53].

2. Conclusions

In conclusion, TMDSC is a powerful thermal analysis technique with the capability of giving more information than conventional DSC. With proper calibration, TMDSC can be used to obtain absolute heat capacities to better than several percent. It also has the potential to yield thermal diffusivity although this measurement is dependent on the nontrivial phase angle calibration. The use of TMDSC to study the reversible melting and crystallization of polymers is anticipated to continue to provide new insights into that field. Its use in the glass transition and structural recovery appears to be more limited, in part because of the limited frequency range available. In the area of thermoset cure, the technique provides additional

information concerning vitrification and phase separation. In all cases, care needs to be taken to insure the experimental conditions of stationarity and linearity are met and caution needs to be used in interpretting data.

References

[1] M. Reading, Trends Polym. Sci. 1 (8) (1993) 248–253.
[2] B. Wunderlich, R. Androsch, M. Pyda, Y.K. Kwon, Thermochim. Acta 348 (1/2) (2000) 181.
[3] M. Reading, D. Elliott, V.L. Hill, J. Therm. Anal. 40 (1993) 949.
[4] G.S. Gill, S.R. Sauerbrunn, M. Reading, J. Therm. Anal. 40 (1993) 931.
[5] E. Verdonck, K. Schaap, L.C. Thomas, Int. J. Pharm. 192 (1999) 3.
[6] U. Jorimann, G. Widmann, R. Riesen, J. Therm. Anal. Calor. 56 (1999) 639.
[7] J.D. Menczel, L. Judovits, J. Therm. Anal. 54 (1998) 419.
[8] B. Wunderlich, Y. Jin, A. Boller, Thermochim. Acta 238 (1994) 277.
[9] M. Reading, D. Elliot, V. Hill, in: Proceedings of the 21st NATAS Conference, 1992, p. 145.
[10] M. Reading, A. Luget, R. Wilson, Thermochim. Acta 238 (1994) 295.
[11] M. Reading, J. Therm. Anal. Calor. 54 (2) (1997) 411.
[12] J.E.K. Schawe, Thermochim. Acta 260 (1995) 1.
[13] N.O. Birge, S.R. Nagel, Phys. Rev. Lett. 54 (25) (1985) 2674.
[14] N.O. Birge, S.R. Nagel, Rev. Sci. Instr. 58 (8) (1987) 1464.
[15] N.O. Birge, Phys. Rev. B 34 (3) (1986) 1631.
[16] J.K. Nielsen, J.C. Dyre, Phys. Rev. B 54 (22) (1996) 15754.
[17] W. Gotze, A. Latz, J. Phys.: Condens. Matter 1 (1989) 4169.
[18] M. Beiner, J. Korus, H. Lockwenz, K. Schroter, E. Donth, Macromolecules 29 (1996) 5183.
[19] E. Donth, M. Beiner, S. Reissig, J. Korus, F. Garwe, S. Vieweg, S. Kahle, E. Hempel, K. Schroter, Macromolecules 29 (1996) 6589.
[20] J. Jackle, Phys. A 162 (1990) 377.
[21] D.W. Oxtoby, J. Chem. Phys. 85 (3) (1986) 1549.
[22] M. Beiner, J. Korus, H. Lockwenz, K. Schroter, E. Donth, Macromolecules 29 (1996) 5183.
[23] Y.-H. Jeong, Thermochim. Acta 304/305 (1997) 67.
[24] J.E.K. Schawe, Thermochim. Acta 304/305 (1997) 111.
[25] J.E.K. Schawe, J. Therm. Anal. 47 (1996) 475.
[26] G.W.H. Höhne, Thermochim. Acta 304/305 (1997) 121.
[27] S.L. Simon, G.B. McKenna, J. Phys. Chem. 107 (20) (1997) 8678.
[28] J.E.K. Schawe, G.W.H. Höhne, J. Therm. Anal. 46 (1996) 893.
[29] R. Urbani, F. Sussich, S. Prejac, A. Cesaro, Thermochim. Acta 304/305 (1997) 359.
[30] M. Merzlyakov, C. Schick, Thermochim. Acta 330 (1999) 55.
[31] J.E.K. Schawe, Thermochim. Acta 271 (1996) 127.
[32] T. Ozawa, K. Kanari, Thermochim. Acta 253 (1995) 183.
[33] I. Hatta, S. Nakayama, Thermochim. Acta 318 (1/2) (1998) 21.
[34] J.E.K. Schawe, E. Bergmann, W. Winter, J. Thermal Anal. 54 (1998) 565.
[35] A. Boller, Y. Jin, B. Wunderlich, J. Therm. Anal. 42 (1994) 307.
[36] P. Claudy, J.M. Vignon, J. Therm. Anal. Calor. 60 (2000) 333.
[37] R. Scherrenberg, V. Mathot, P. Steeman, J. Therm. Anal. 54 (1998) 477.
[38] C.R. Snyder, F.I. Mopsik, J. Chem. Phys. 110 (2) (1999) 1106.
[39] M.L. Di Lorenzo, B. Wunderlich, J. Therm. Anal. Calor. 57 (1999) 459.
[40] B. Wunderlich, A. Boller, I. Okazaki, S. Kreitmeier, Thermochim. Acta 283 (1996) 143.
[41] M. Varma-Nair, B. Wunderlich, J. Therm. Anal. 46 (1996) 879.
[42] B. Wunderlich, A. Boller, I. Okazaki, K. Ishikiriyama, Thermochim. Acta 304/305 (1997) 125.
[43] G.W.H. Höhne, N.B. Shenogina, Thermochim. Acta 310 (1998) 47.
[44] I. Hatta, A.A. Minakov, Thermochim. Acta 330 (1999) 39.
[45] R. Androsch, M. Pyda, H. Wang, B. Wunderlich, J. Therm. Anal. Calor. 61 (3) (2000) 661.
[46] S.L. Simon, G.B. McKenna, J. Reinforced Plast. Composites 18 (6) (1999) 559.
[47] B. Schenker, F. Stager, Thermochim. Acta 304/305 (1997) 219.
[48] F.U. Buehler, J.C. Seferis, Themochim. Acta 348 (2000) 161.
[49] J.E.K. Schawe, W. Winter, Thermochim. Acta 298 (1997) 9.
[50] S.A. Knopp, S.L. Nail, J. Therm. Anal. Calor. 60 (2000) 319.
[51] S.L. Simon, G.B. McKenna, Thermochim. Acta 307 (1997) 1.
[52] A.A. Lacey, C. Nikolopoulos, M. Reading, J. Therm. Anal. 50 (1997) 279.
[53] G.W.H. Höhne, M. Merzlyakov, C. Schick, Thermochim. Acta, submitted for publication.
[54] F.U. Buehler, Ph.D. Dissertation, Univeristy of Washington, Washington, 2000.
[55] G.W.H. Höhne, Thermochim. Acta 330 (1999) 45.
[56] K. Kanari, T. Ozawa, Thermochim. Acta 304/305 (1997) 201.
[57] J. Cao, Thermochim. Acta 325 (1999) 101.
[58] S.M. Marcus, R.L. Blaine, Thermochim. Acta 243 (1994) 231.
[59] M. Merzlyakov, C. Schick, Thermochim. Acta, accepted for publication.
[60] G.B. McKenna, in: C. Booth, C. Price (Eds.), Comprehensive Polymer Science, Vol. 2, Polymer Properties, Pergamon, Oxford, 1989, Chapter 2.
[61] I. Hodge, J. Non-Cryst. Solids 169 (1994) 211.
[62] J.M. Hutchinson, Prog. Polym. Sci. 20 (1995) 703.

[63] G.B. McKenna, S.L. Simon, The glass transition: its measurement underlying physics, in: S.Z.D. Cheng (Ed.), Handbook of Thermal Analytical Calorimeter, Vol. 3, Elsevier, Amsterdam, in press.
[64] J.E.K. Schawe, Thermochim. Acta 261 (1995) 183.
[65] A. Boller, C. Schick, B. Wunderlich, Thermochim. Acta 266 (1995) 97.
[66] A. Boller, I. Okazaki, B. Wunderlich, Thermochim. Acta 284 (1996) 1.
[67] B. Wunderlich, A. Boller, I. Okazaki, S. Kreitmeier, J. Therm. Anal. 47 (1996) 1013.
[68] A. Hensel, J. Dobbertin, J.E.K. Schawe, A. Boller, C. Schick, J. Therm. Anal. 46 (1996) 935.
[69] J.M. Hutchinson, S. Montserrat, J. Therm. Anal. 47 (1996) 103.
[70] K.L. Jones, I. Kinshott, M. Reading, A.A. Lacey, C. Nikolopoulos, H.M. Pollock, Thermochim. Acta 304/305 (1997) 187.
[71] J.M. Hutchinson, Thermochim. Acta 324 (1998) 165.
[72] S. Montserrat, J. Therm. Anal. Calor. 59 (2000) 289.
[73] S.E.B. Petrie, J. Polym. Sci. A2 10 (1972) 1255.
[74] O.S. Narayanaswamy, J. Am. Ceram. Soc. 54 (1971) 491.
[75] C.T. Moynihan, P.B. Macedo, C.J. Montrose, P.K. Gupta, M.A. DeBolt, J.F. Dill, B.E. Dom, P.W. Drake, A.J. Easteal, P.B. Elterman, R.P. Moeller, H. Sasabe, J.A. Wilder, Ann. NY Acad. Sci. 279 (1976) 15.
[76] S.L. Simon, G.B. McKenna, Thermochim. Acta 348 (2000) 77.
[77] J.E.K. Schawe, S. Theobald, J. Non-Crsyt. Solids 235–237 (1998) 496.
[78] B. Wunderlich, I. Okazaki, J. Therm. Anal. 49 (1997) 57.
[79] S. Weyer, C. Schick, Thermochim. Acta accepted for publication.
[80] D.J. Hourston, et al., Polymer 37 (1996) 43
[81] J.M. Hutchinson, A.B. Toon, Z. Jiang, Thermochim. Acta 335 (1999) 27.
[82] N.A. Bailey, J.N. Hay, D.M. Price, Thermochim. Acta, submitted for publication.
[83] J.M. Hutchinson, S. Montserrat, Thermochim. Acta 304 (1997) 257.
[84] J.E.K. Schawe, G.R. Strobl, Polymer 39 (16) (1998) 3745.
[85] G.W.H. Höhne, Thermochim. Acta 330 (1999) 93.
[86] B. Wunderlich, I. Okazaki, K. Ishikiriyama, A. Boller, Thermochim. Acta 324 (1998) 77.
[87] B. Wunderlich, A. Boller, I. Okazaki, K. Ishikiriyama, W. Chen, M. Pyda, J. Pak, I. Moon, R. Androsch, Thermochim. Acta 330 (1999) 21.
[88] K. Ishikiriyama, A. Boller, B. Underlich, J. Therm. Anal. 40 (1997) 47.
[89] B. Wunderlich, Macromolecular Physics, Vol. 3, Academic Press, New York, 1976.
[90] M. Reading, A. Luget, R. Wilson, Thermochim. Acta 238 (1994) 295.
[91] M. Nishikawa, Y. Saruyama, Thermochim. Acta 267 (1995) 75.
[92] I. Okazaki, B. Wunderlich, Macromolecules 30 (1997) 1758.
[93] K. Ishikiriyama, B. Wunderlich, J. Polym. Sci., Part B, Polym. Phys. 35 (1997) 1977.
[94] K. Ishikiriyama, B. Wunderlich, Macromolecules 30 (1997) 4126.
[95] M. Pyda, A. Boller, J. Grebowicz, H. Chuah, B.V. Lebedev, B. Wunderlich, J. Part B, Polym. Phys. 36 (1998) 2499.
[96] J.E.K. Schawe, E. Bergmann, Thermochim. Acta 304/305 (1997) 179.
[97] C. Schick, M. Merzlyakov, B. Wunderlich, Polym. Bull. 40 (1998) 297.
[98] A. Wurm, M. Merzlyakov, C. Schick, Coll. Polym. Sci. 276 (1998) 289.
[99] M.C. Righetti, Thermochim. Acta 330 (1999) 131.
[100] A. Toda, C. Tomita, M. Hikosaka, Y. Saruyama, Polymer 39 (21) (1998) 5093.
[101] W. Chen, M. Dadmun, G. Zhang, A. Boller, B. Wunderlich, Thermochim. Acta 324 (1998) 87.
[102] A. Toda, C. Tomita, M. Hikosaka, Y. Saruyama, Thermochim. Acta 324 (1998) 95.
[103] A. Toda, T. Arita, C. Tomita, M. Hikosaka, Thermochim. Acta 330 (1999) 75.
[104] J.E.K. Schawe, W. Winter, Themochim. Acta 330 (1999) 85.
[105] J.E.K. Schawe, G.R. Strobl, Polymer 39 (16) (1998) 3745.
[106] A. Toda, T. Oda, M. Hikosaka, Y. Saruyama, Polymer 38 (1) (1997) 231.
[107] A. Toda, T. Oda, M. Hikosaka, Y. Saruyama, Thermochim. Acta 293 (1997) 47.
[108] A. Toda, C. Tomita, M. Hikosaka, Y. Saruyama, Polymer 39 (21) (1998) 5093.
[109] R. Scherrenberg, V. Mathot, A. Van Hemelrijck, Thermochim. Acta 330 (1999) 3.
[110] C. Schick, M. Merzlyakov, A. Minakov, A. Wurm, J. Therm. Anal. Calor. 59 (2000) 279.
[111] J.K. Gillham, Polym. Eng. Sci. 26 (20) (1986) 1429.
[112] S.L. Simon, J.K. Gillham, J. Appl. Polym. Sci. 47 (1993) 461.
[113] G. Van Assche, A. Van Hemelrijck, H. Rahier, B. Van Mele, Thermochim. Acta 268 (1995) 121.
[114] S. Montserrat, I. Cima, Thermochim. Acta 330 (1999) 189.
[115] G. Van Assche, A. Van Hemelrijck, H. Rahier, B. Van Mele, Thermochim. Acta 286 (1996) 209.
[116] J.K. Gillham, J.B. Enns, Trends Polym. Sci. 2 (12) (1994) 406.
[117] A. Van Hemelrijck, B. Van Mele, J. Therm. Anal. 49 (1997) 437.
[118] S. Swier, G. Van Assche, A. Van Hemelrijck, H. Rahier, E. Verdonck, B. Van Mele, J. Therm. Anal. 54 (1998) 585.
[119] S.B. Van Mele, Thermochim. Acta 330 (1999) 175.
[120] I. Alig, W. Jenninger, J.E.K. Schawe, Thermochim. Acta 330 (1999) 167.
[121] W. Jenninger, J.E.K. Schawe, I Alig, Polymer 41 (2000) 1577.
[122] G. Van Assche, E. Verdonck, B. Van Mele, J. Therm. Anal. 59 (2000) 305.
[123] C. Tomasi, P. Mustarelli, E. Quartarone, R. Pepi, Thermochim. Acta 304/305 (1997) 353.
[124] M. Song, D.J. Hourston, H.M. Pollock, F.U. Schafer, A. Hammiche, Thermochim. Acta 304/305 (1997) 335.
[125] D.J. Hourston, M. Song, F.-U. Schafer, H.M. Pollock, A. Hammiche, Thermochim. Acta 324 (1998) 109.

[126] M. Song, D.J. Hourston, M. Reading, H.M. Pollock, A. Hammiche, J. Therm. Anal. Calor. 56 (1999) 991.
[127] G. Pompe, U. Schulze, J. Hu, J. Pionteck, G.W.H. Höhne, Thermochim. Acta 337 (1999) 179.
[128] Y.Y. Cheng, M.V. Brillart, P. Cebe, Thermochim. Acta 304/305 (1997) 369.
[129] A. Hensel, C. Schick, Thermochim. Acta 304/305 (1997) 229.
[130] T. Ozawa, K. Kanari, Thermochim. Acta 253 (1995) 183.
[131] A. Marini, V. Berbenni, G. Bruni, A. Maggioni, M. Villa, J. Therm. Anal. Calor. 56 (1999) 699.
[132] M. Reading, R. Luyt, J. Chem. Anal. Calor. 54 (1998) 535.
[133] S. Weyer, A. Hensel, C. Schick, Thermochim. Acta 304/305 (1997) 267.
[134] Z. Jiang, C.T. Imrie, J.M. Hutchinson, Thermochim. Acta 314 (1998) 1.
[135] Z. Jiang, C.T. Imrie, J.M. Hutchinson, Thermochim. Acta 336 (1999) 27.